Journal of Physical Science, Vol. 30(1), 81–97, 2019

Mechanical Strength and Corrosion Rate of Aluminium Composites (Al/SiO_2): Nanoparticle Silica (NPS) as Reinforcement

Munasir,[1*] Triwikantoro,[2] Mochamad Zainuri,[2] Ralph Bäßler[3] and Darminto[2]

[1]Department of Physics, Faculty of Mathematics and Sciences,
Universitas Negeri Surabaya (UNESA),
Jl. Ketintang, Surabaya 60231, Indonesia
[2]Department of Physics, Faculty of Mathematics and Sciences,
Institut Teknologi Sepuluh, Nopember (ITS), Kampus ITS,
Jl. Arif Rahman Hakim, Sukolilo, Surabaya 60111, Indonesia
[3]BAM Federal Institute for Materials Research and Testing, Department Safety of Structure (Dpt.7), Unter den Eichen 87, 12205 Berlin, Germany

[*]Corresponding author: munasir_physics@unesa.ac.id

Published online: 25 April 2019

To cite this article: Munasir et al. (2019). Mechanical strength and corrosion rate of aluminium composites (Al/SiO_2): Nanoparticle silica (NPS) as reinforcement. *J. Phys. Sci.*, 30(1), 81–97, https://doi.org/10.21315/jps2019.30.1.7

To link to this article: https://doi.org/10.21315/jps2019.30.1.7

ABSTRACT: *The fabrication and characteristics of amorphous silica reinforced Al matrix composites are studied in this paper. The major starting materials were commercial Al powder and extracted nanoparticle SiO_2 (NPS) powder from Indonesian silica sands. Two different active solutions, namely N-butanol and tetramethylammonium hydroxide (TMAH), were introduced during synthesis. Characterisations in terms of physical, mechanical, microstructural and corrosion rate examinations were also employed. Introducing the SiO_2 nanoparticles into the Al matrix has decreased the density and increased the porosity of the composites. The addition of N-butanol into Al/SiO_2 ($Al/SiO_2(B)$) led to broader and lower X-ray diffraction profiles than the addition of TMAH ($Al/SiO_2(T)$). From the microstructural analysis, we found that the SiO_2 particles enter and agglomerate into the opening gap of the Al sheets. Furthermore, yield strength, ultimate compression strength and modulus of elasticity tended to reduce the addition of SiO_2. The corrosion rate of $Al/SiO_2(T)$ was lower than that of $Al/SiO_2(B)$ composites.*

Keywords: Aluminium, silica (SiO_2), Al/SiO_2 composite, mechanical strength, corrosion rate

1. INTRODUCTION

Aluminium is one of the most popular non-ferrous metal matrix composites (MMCs) due to its excellent characteristics in terms of low density, good corrosion, high acid resistance, and high thermal and electrical conductivities.[1,2] Aluminium-based MMCs with Al_2O_3 and SiC reinforcements have enhanced some important material properties like tensile strength, elastic modulus, hardness, wear resistance, thermal conductivity and corrosion resistance.[3,4]

Latest studies reveal that SiO_2 has become a potential reinforcement in aluminium-based MMCs due to its prospective applications for automotive, defence, chemical, and oil and natural gas industries.[6–9] Selecting SiO_2 as the reinforcement in aluminium-based MMCs improves their impact strength, hardness, porosity, wear and corrosion resistance, but reduces the ductility, toughness, tensile strength, elastic modulus and thermal conductivity.[6–7,10–14] Concerning corrosion resistant property, a potentiodynamic polarisation system has been used to investigate corrosion characteristics of Al and its alloys, Al/SiC_p (6061Al-SiC) and Al-fly ash.[15,17–19] Their corrosion rate increases along with the increasing temperature, medium concentration and profile of pitting corrosion in the surface.

This study deals with the simple approach of producing Al/SiO_2 composites prepared by two different active solutions, i.e., N-butanol and tetra-methyl-ammonium-hydroxide (TMAH), as well as their microstructural and mechanical characteristics. Furthermore, the corrosion rate of the composites will also be studied. To the best of our knowledge, a comprehensive examination of the properties of amorphous nano-silica-reinforced aluminium employing various active solutions as media mixing matrix and filler has, so far, has rarely been reported.

2. EXPERIMENTAL

The raw materials were Al powders (Merck) and extracted amorphous SiO_2 powders with an average crystallite size of around 35 nm that were prepared from natural silica sands.[20] The elemental contents of those raw materials are detailed in Table 1. Al/SiO_2 composites were synthesised with varying content of SiO_2 (in vol.%): 0, 5, 10, 15, 20, 25 and 30 by simply mixing Al and SiO_2 in two different active solutions, namely N-butanol and TMAH, for 2 h. The mixtures were then dried at 120°C for 12 h. The dried powders were uniaxially pressed in a metal die by applying a pressure of 200 N m^{-2} to produce cylindrical samples with a thickness of 10 mm and a diameter of 13 mm. Heat treatment was given to the

samples by pre-sintering at 200°C for 0.75 h, followed by vacuum sintering at 500°C for 2 h. The sintered samples were labeled as Al/SiO_2(B) and Al/SiO_2(T), standing respectively for N-butanol and TMAH treatments.

Table 1: Elemental contents of Al and nano-SiO_2.

Powders	Element (wt.%)										
	Al	Si	P	Ca	Ba	V	Cr	K	Fe	Ni	Others
Al	98.10	0.00	0.68	0.41	0.08	0.06	0.02	0.00	0.36	0.02	< 0.01
SiO_2	0.00	97.30	0.00	1.00	0.00	0.05	0.00	0.16	1.08	0.00	< 0.01

Phase compositions within the composites were evaluated using Cu-Kα radiation X-ray diffraction (XRD) data. Elemental mapping and microstructures were analysed by scanning electron microscopy and energy dispersive spectrometry (SEM-EDX) module. Density and porosity were measured using the Archimedes principle, while the mechanical properties were investigated through a compression test. The corrosion rate was studied by potentiodynamic polarisation using stainless steel as the calculating electrode, Al/SiO_2 composite as working electrode, and Ag/AgCl as a reference electrode. ANOVA analysis was employed to evaluate the Tafel curve using Butler-Volmer mathematical expression, and polarisation resistance was calculated using the Stern-Geary equation.[15] The Tafel analysis yielded some important corrosion parameters, namely, the calculated corrosion potential ($E_{cor,Calc}$), the observed corrosion potential ($E_{cor,Obs}$), corrosion current (i_{corr}), corrosion current density (j_{Corr}), polarisation resistance (R_p) and corrosion rate (V_{Corr} (*mm/y*)).[16–18]

3. RESULTS AND DISCUSSION

3.1 Mechanical Properties

Figure 1 shows the characteristic density and porosity of the prepared composites. In general, for samples with 5% to 20% SiO_2 content, the density decreased and therefore, the porosity increased. This was in line with the previous report.[14] The lowest density (the highest porosity) was shown by the 20% SiO_2 sample, while the highest density (the lowest porosity) was shown by 5% SiO_2 sample, which proved to be the best among the samples. Figure 1 illustrates that there is no strong influence in employing N-butanol and TMAH solutions as mixing media during the sample preparation.

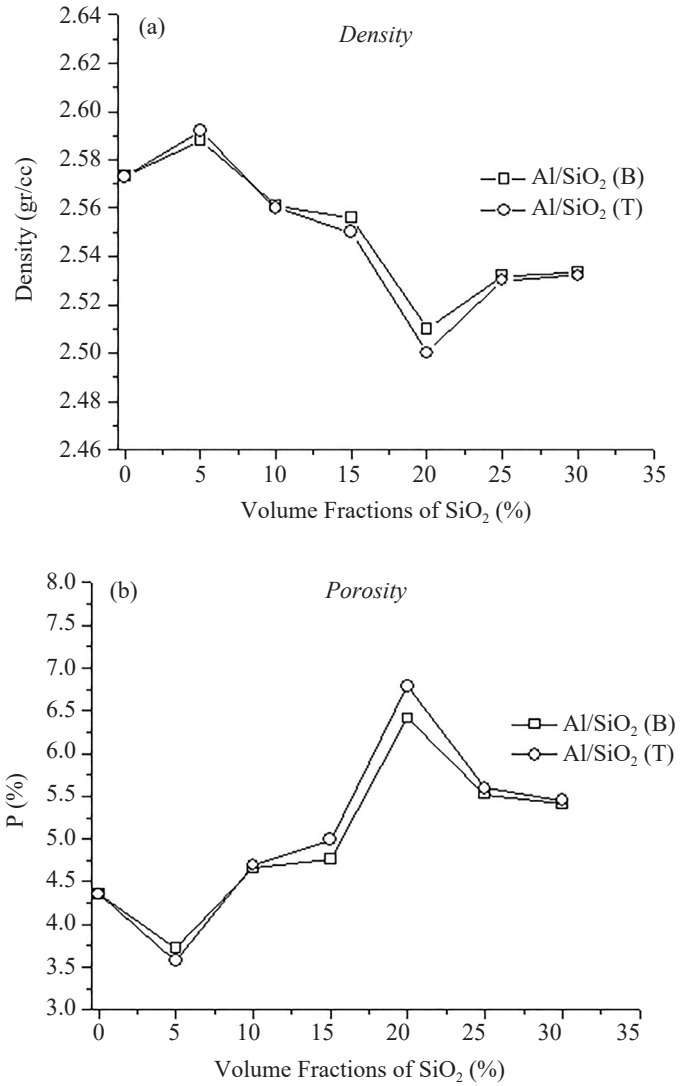

Figure 1: Plots of (a) density, and (b) porosity of Al-SiO_2 composites.

Measured modulus of elasticity (E_c) of the Al/SiO_2 composite is given in Figure 2(a). The sample with 5% SiO_2 content demonstrated the highest E_c, and the sample with 5% SiO_2 showed the lowest E_c. The decreasing trend of E_c may be due to individual E_c of both Al and nano-SiO_2, respectively having values of about 69 GPa and 72 Gpa.[6,7] As we may observe in Figure 2, the modulus of elasticity does not merely decrease; it increases when the SiO_2 content exceeds 20%. This behaviour can be explained by the rule of mixture principle in which the upper bound and lower bound for the two components, Al and SiO_2 are relatively closer.[21]

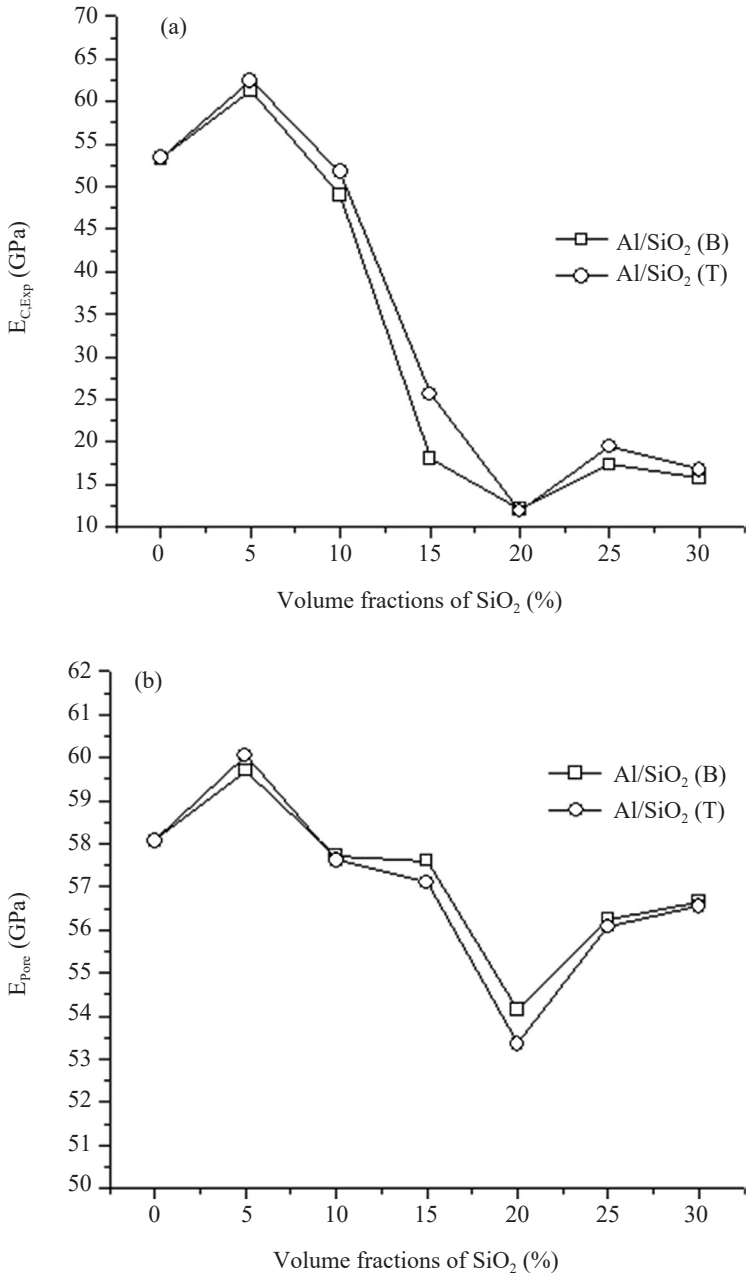

Figure 2: Plots of (a) measured, and (b) calculated modulus of elasticity of Al/SiO_2.

Nevertheless, the porosity should be considered for evaluating the modulus of elasticity.[8,22] Since we introduced SiO_2 as discontinuous reinforcement, the modulus of elasticity with porosity involvement can be best computed using Sprigg's equation, where E_{pore} and E_o are respectively the theoretical moduli of elasticity with and without porosity considerations, b is a constant for the filler ratio factor having value of around 3.95, and P is porosity. As it is well known, the E_o can be calculated using the Halpin-Tsai expression.[21,22]

$$E_{pore} = E_o e^{-bP} \tag{1}$$

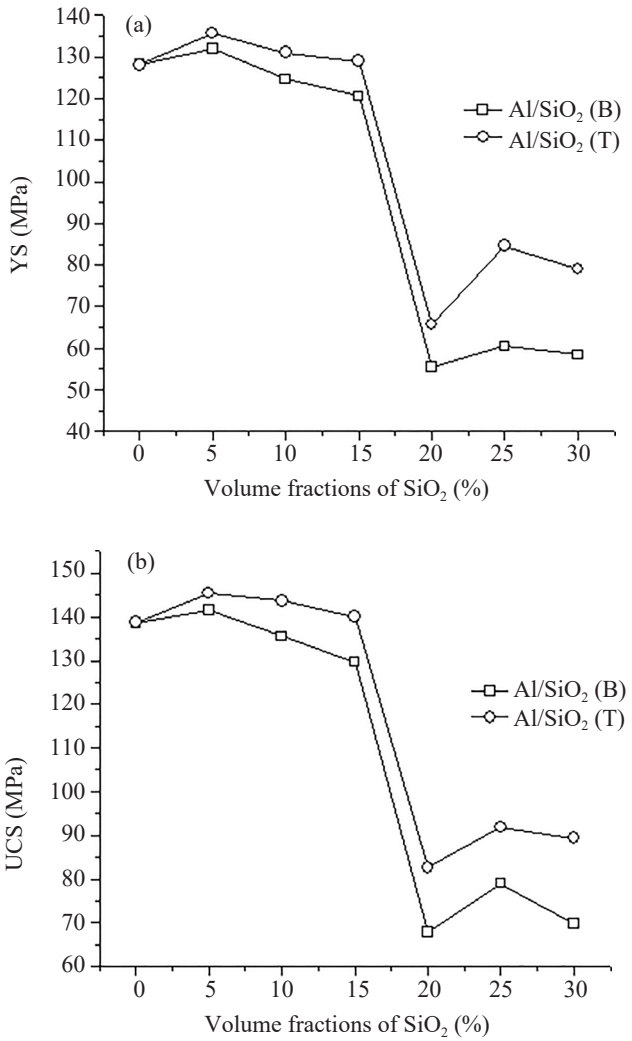

Figure 3: Plots of (a) yield strength, and (b) ultimate compression strength of Al/SiO_2.

In Figure 2(b), the E_{pore} characteristic of the composites is seen as showing the same trends but having larger values as compared to the E_c characteristic. These trends accord well with another report introducing nano-sized SiO_2 into the Al matrix, which would enhance the modulus of elasticity up to about 14 Gpa.[7] Meanwhile, for micron-sized SiO_2, reinforcement may give only around 0.240 Gpa.[11] Our present study exhibited that the maximum modulus of elasticity attained was 61.28 GPa and 62.43 GPa respectively for Al/SiO_2(B) and Al/SiO_2(T) samples with 5% SiO_2. This finding signifies that the addition of 5% SiO_2 leads to the most superior Al/SiO_2 composite in terms of its modulus of elasticity.[21,23] The characteristics of yield strength (YS) and ultimate compression strength (UCS) of Al/SiO_2 are given in Figure 3, and they agreed with other investigations.[7,11,14] Both UCS and YS of Al/SiO_2(T) were slightly greater than those of Al/SiO_2(B), implying that the use of TMAH may enable more homogenous distribution of SiO_2 within the composites.

3.2 Microstructures

Figures 4 and 5 show the representative XRD spectra for Al/SiO_2(B) and Al/SiO_2(T) composites after their phase identification. From Figure 4, we can see that only Al (reference code 00-004-0787) and γ-Al_2O_3 (00-002-1420) are present in all composites. Figure 2 also clarifies the noncrystalline SiO_2 content through the absence of any SiO_2 peak, implying that the whole treatment in all the processes did not transform the structure of silica from amorphous to crystalline state. The occurrence of γ-Al_2O_3, especially in Figure 5, indicates that γ-Al_2O_3 is likely to form due to sintering Al/SiO_2 mixtures. OH^- ions can easily react with Al powders forming aluminium hydroxide (γ-$Al(OH)_3$), which in turns transforms into γ-Al_2O_3 after sintering.[24–28]

Adding N-butanol and TMAH as the active solutions along with Al/SiO_2 synthesis strongly affects the crystalline states and sizes of the composites. More amorphous state and smaller crystallite size, which are qualitatively indicated by the broader and lower XRD peaks, are obtained by Al/SiO_2(T) rather than Al/SiO_2(B) (see Figures 4 and 5). This evidence indicates that the addition of TMAH may reduce the dominance of Al in the composites. Also, more γ-Al_2O_3 formed in Al/SiO_2(T).

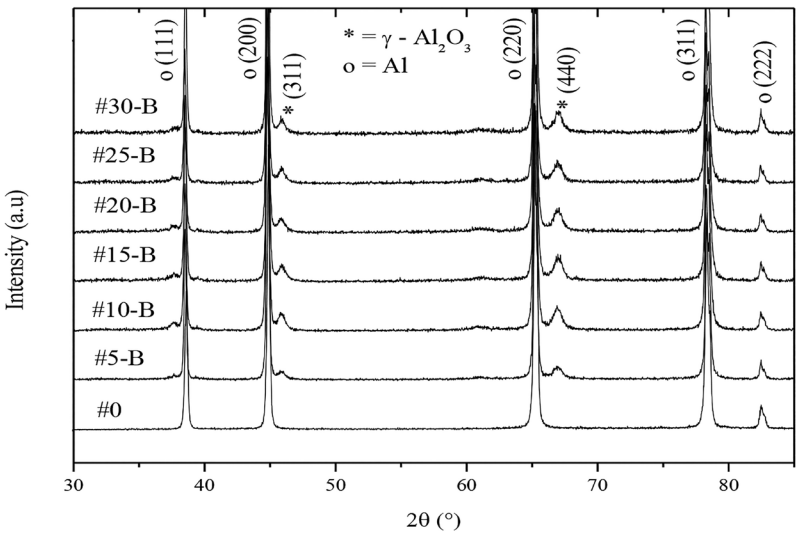

Figure 4: XRD profiles for Al/SiO_2(B) composites: #0 for pure Al; #5-B for 5% SiO_2; #10-B for 10% SiO_2; and so forth. The letter B indicates the N-butanol addition during synthesis.

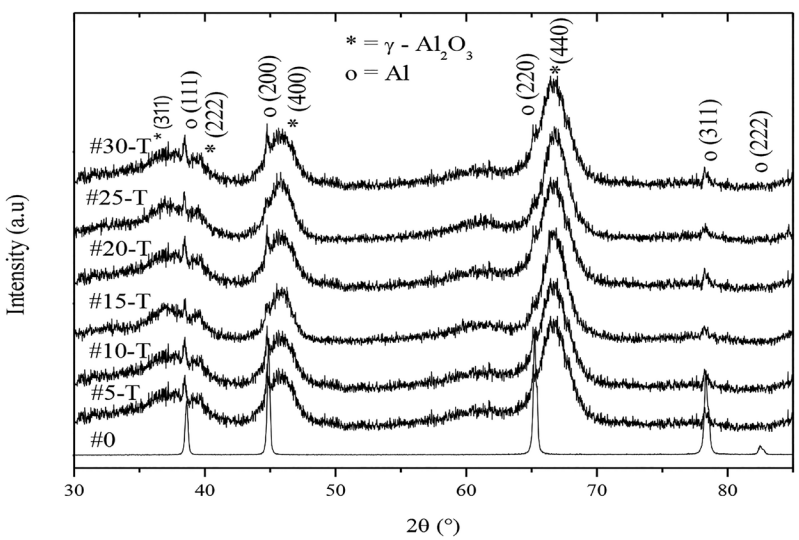

Figure 5: XRD profiles for Al/SiO_2(T) composites: #0 for pure Al; #5-T for 5% SiO_2; #10-T for 10% SiO_2; and so forth. The letter T indicates the TMAH addition during synthesis.

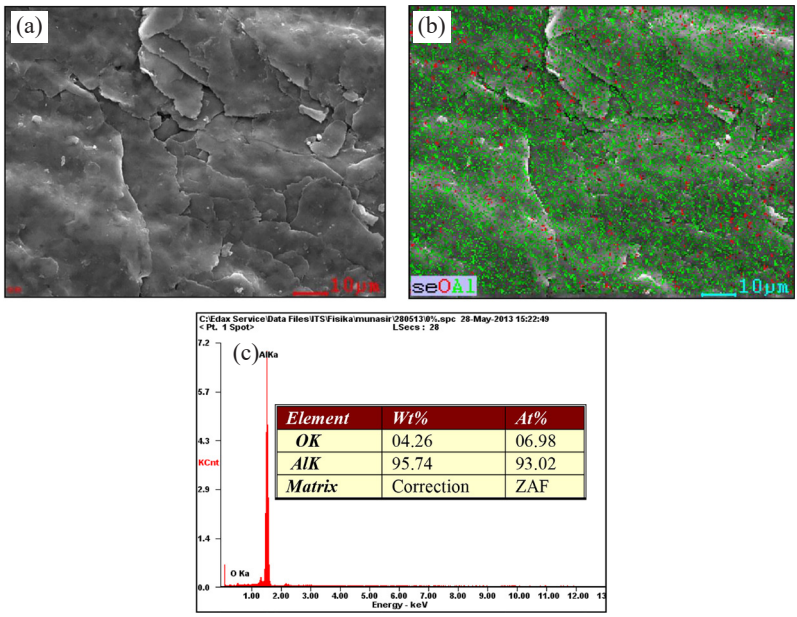

Figure 6: Illustrations of (a) micrographical, and (b–c) elemental mapping of Al observed using 1000X magnification.

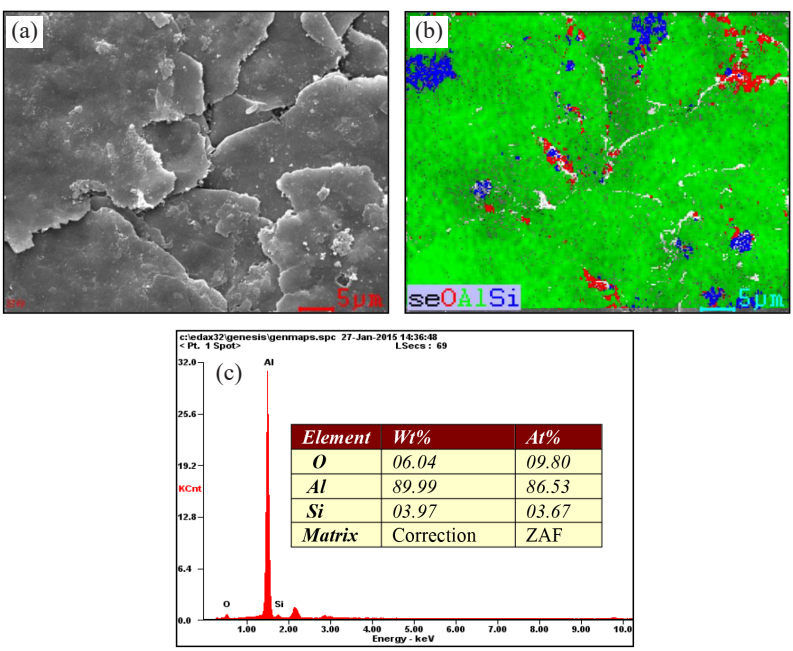

Figure 7: Illustrations of (a) micrographical, and (b–c) elemental mapping of Al/SiO_2(B) composite with 5% SiO_2 observed using 1000X magnification.

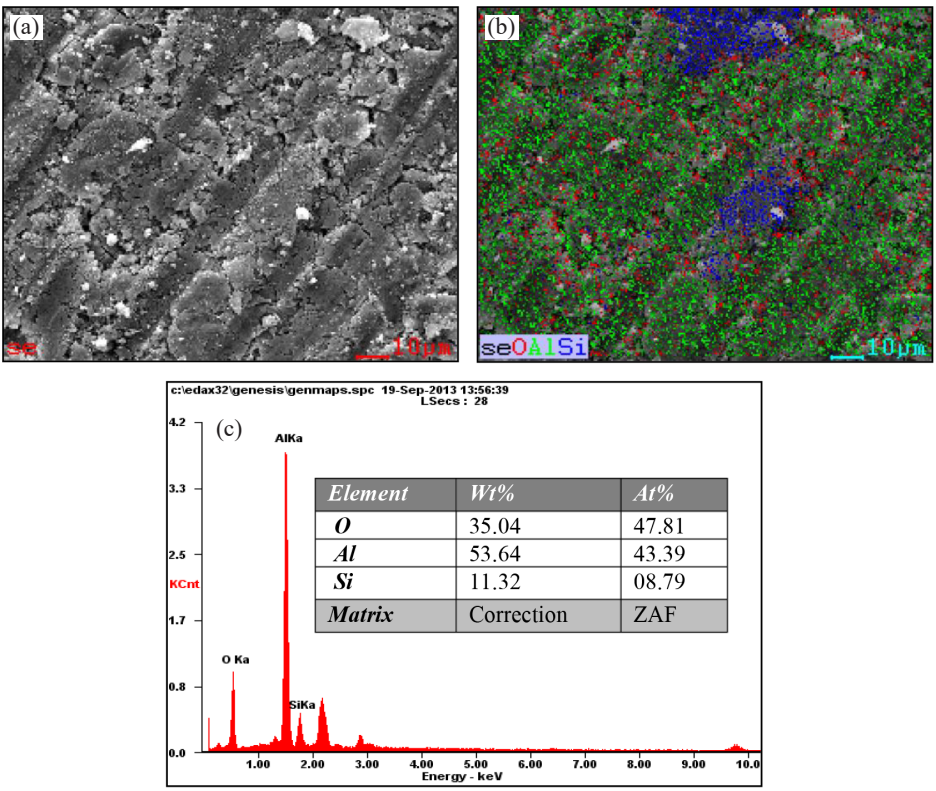

Figure 8: Illustrations of (a) micrographical, and (b–c) elemental mapping of Al/SiO_2(T) composite with 5% SiO_2 observed using 1000X magnification.

Figures 6, 7 and 8 show respectively the micrographic images as well as the elemental mapping for pure Al, 5% SiO_2 in Al/SiO_2(B), and in Al/SiO_2(T). In the figures, it is seen that Al appears like sheets, with SiO_2 particles entering and agglomerating into the opening gaps in the sheets. Grains of Si, Al and O elements are present. The sheets of Al appear very clearly in Figure 6. Also, larger and more homogenous grains of Al are found in Figure 7(a) as compared to Figure 8(a). In Figure 8(b), the elemental mapping viewpoint, more of γ-Al_2O_3 can be detected. Different elemental contents of the samples of Al/SiO_2(B) and Al/SiO_2(T) with 5% SiO_2 are shown in Figures 7(c) and 8(c). These results seem to support the XRD data as previously discussed.

The more detailed micrographs of non-homogenous distribution of amorphous SiO_2 within Al matrix are presented in Figure 9 (#25-B sample). Even supposing that SiO_2 has a large specific surface area due to its nano-sized structure, its agglomeration remains observed, shown in Figure 9(c). The distribution of the

reinforcement, in this case SiO_2, is affected by its size.[1,7,21] Also, the large specific surface area of SiO_2 plays an important role in the interfacial bonding of the composite.[8] In Figure 9, the presence of interfacial bonding between Al and SiO_2 with sphere-plane characteristic is also illustrated. This type of bonding contributes to the enhanced mechanical properties of the composites. The elemental mapping in the selected grain and the grain boundaries of Al/SiO_2(B) with 15% SiO_2 (#15-B sample) are shown in Figure 10. In terms of wt%, the highest and the lowest Al contents are found respectively in the areas 1 and 3, which are simultaneously correlated to the lowest and the highest Si contents respectively. Again, Figures 9 and 10 very well support the XRD data, especially as the evidence of the presence of the γ-Al_2O_3 phase.

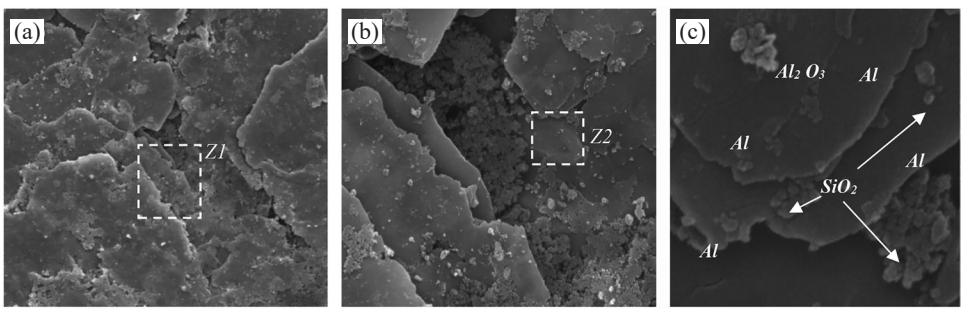

Figure 9: SEM micrography for Al/SiO_2(B) with 25% SiO_2 (#25-B) using (a) 5,000X magnification, (b) zooming in Z1 area with 20,000X magnification, and (c) zooming in Z2 area with 150,000X.

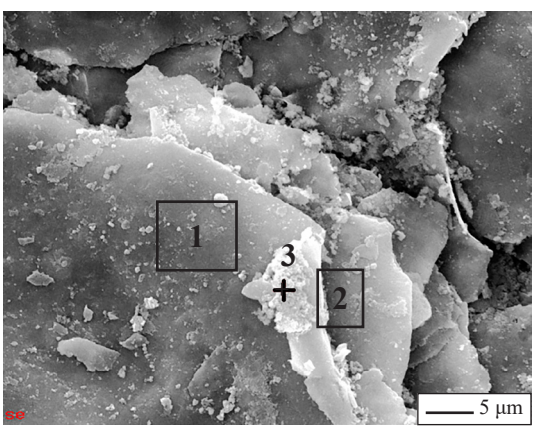

Area	Element	Wt%	At%
1	O	12,40	19,32
	Al	81,77	75,51
	Si	5,83	5,17
2	O	17,21	26,01
	Al	76,81	68,84
	Si	5,98	5,15
3	O	25,21	36,41
	Al	61,28	52,48
	Si	13,51	11,11

Figure 10: EDS elemental mapping of Al/SiO_2(B) with 15% SiO_2 (#15-B sample) in grain boundaries. The elemental content was observed from areas specified (1, 2, 3) on the figure.

3.3 Corrosion Rate

The results from the Tafel curve analysis and its parameters for Al/SiO_2 composites with volume fraction 0% SiO_2 or bulk-pure Al are represented in Figure 11 and Table 2. The corrosion parameters obtained from the Tafel curve analysis for Al/SiO_2 composites are shown in Table 3. The corrosion rate and the current density were calculated using the Stern-Geary equation:[27]

$$j_{corr} = \frac{\beta_a \beta_b}{2.303 R_p (\beta_a + \beta_b)} \tag{2}$$

and

$$V_{Corr} = C J_{Corr} W_{eq} \tag{3}$$

where C is a constant that labels the corrosion rate units divided by the specimen density and area, and W_{eq} is equivalent to the weight of the material.

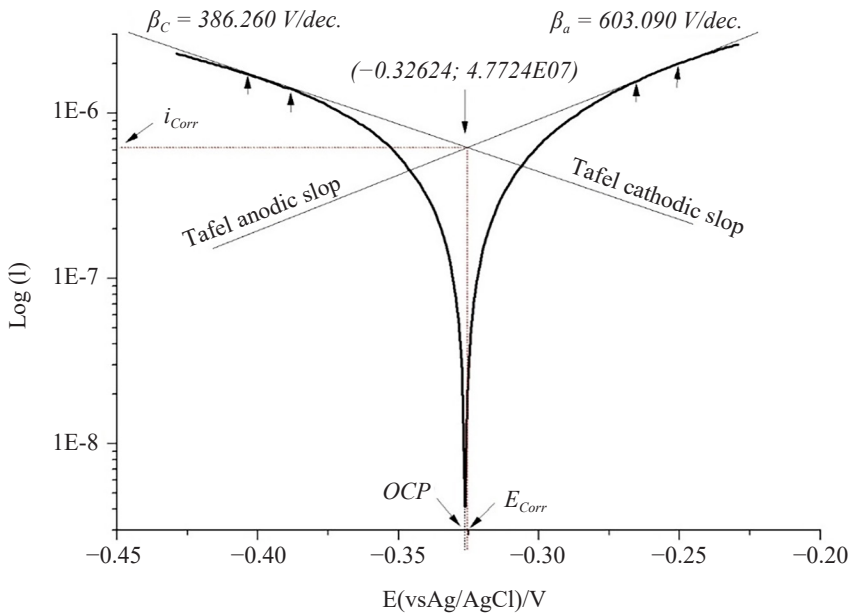

Figure 11: Tafel curve for Al/SiO_2 (#0 sample) composites from potentiodynamic polarisation test with 1M NaCl medium at room temperature.

The corrosion rates of all composites (#0 sample and Al/SiO_2 samples) can be seen in Figure 12. The corrosion rates of Al/SiO_2(B) and Al/SiO_2(T) clearly have different trends. The corrosion rates for both types of composites, Al/SiO_2(B) and Al/SiO_2(T), increase with increasing SiO_2 content. Introducing TMAH during

the synthesis leads to lower corrosion rates than those produced by N-butanol. In comparison, the corrosion rates of Al/SiO_2(T) with incorporation of 0%, 5%, 10%, 15%, 20%, 25% and 30% of SiO_2, were respectively 0.05504 mm y^{-1}, 0.03461 mm y^{-1}, 0.05749 mm y^{-1}, 0.16936 mm y^{-1}, 0.19117 mm y^{-1}, 0.15807 mm y^{-1} and 0.10831 mm y^{-1}. Meanwhile, the corrosion rates of Al/SiO_2(B) with an addition of 0%, 5%, 10%, 15%, 20%, 25% and 30% of SiO_2, were 0.05504 mm y^{-1}, 0.03968 mm y^{-1}, 0.09975 mm y^{-1}, 1.61440 mm y^{-1}, 1.7020 mm y^{-1}, 1.434 mm y^{-1} and 1.3246 mm y^{-1}, respectively. This implies that the presence of 20% of SiO_2 in the Al/SiO_2(B) (V_{Corr} ≈ 1.7020 mm y^{-1}) is roughly ten times less corrosive than in the Al/SiO_2(T) (V_{Corr} ≈ 0.19117 mm y^{-1}). Furthermore, the Al/SiO_2 for the volume fraction of 5% of SiO_2 not only has a higher corrosion resistance than bulk pure-aluminium (#0), but also the most excellent mechanical properties, i.e., modulus elasticity, yield strength, and ultimate compression strength (Figures 2 and 3).

Table 2: Data of Tafel analysis with NOVA software for Al/SiO_2 sample (#0, example).

Parameter Tafel analysis	Result
Open circuit potential, OCP	–0.329 V
Coef. of Tafel anodic, β_a	603.090 mV dec^{-1}
Coef. of Tafel cathodic, β_c	386.260 mV dec^{-1}
E_{Corr} calculation	–325.240 mV
E_{Corr} observation	–326.210 mV
j_{Corr}	4.73680 µA cm^{-2}
i_{corr}	2.430 µA
Corrosion rate, V_{Corr}	0.055042 mm y^{-1}
Polarisation resistance	42.0800 kΩ
E begin	–399.020 mV
E end	–256.960 mV
x^2	3.7607E-15
Iterations	60
Sample parameters:	
Density	7.86 g cm^{-2}
Equivalent weight	27.925 g mol^{-1}
Surface area	0.513 cm^2
Number of significant digits	5

Also, both Al/SiO_2(T) and Al/SiO_2(B) show nearly the same value of corrosion rate at 5% SiO_2 and demonstrate the best reductive characteristic in chloride-based environments. But, the presence of 5% of SiO_2 in the Al/SiO_2(T) has a corrosion resistance stronger (V_{Corr} ≈ 0.03461 mm y^{-1}) than in the Al/SiO_2(B) (V_{Corr} ≈ 0.03968 mm y^{-1}). It is because of the more amount of γ-Al_2O_3 phase

formed at Al/SiO_2(T) than Al/SiO_2(B) (EDX or elemental mapping shown in Figures 7(b and c) and 8 (b and c); and XRD datas (Figures 4 and 5). Particles of amorphous silica fill the gaps among the Al layers to prevent corrosive agents from terminating the composites. Also, more SiO_2 aggregates initiate the presence of agglomeration (Figure 9c), which in turn reduces corrosion rates (Figure 12).

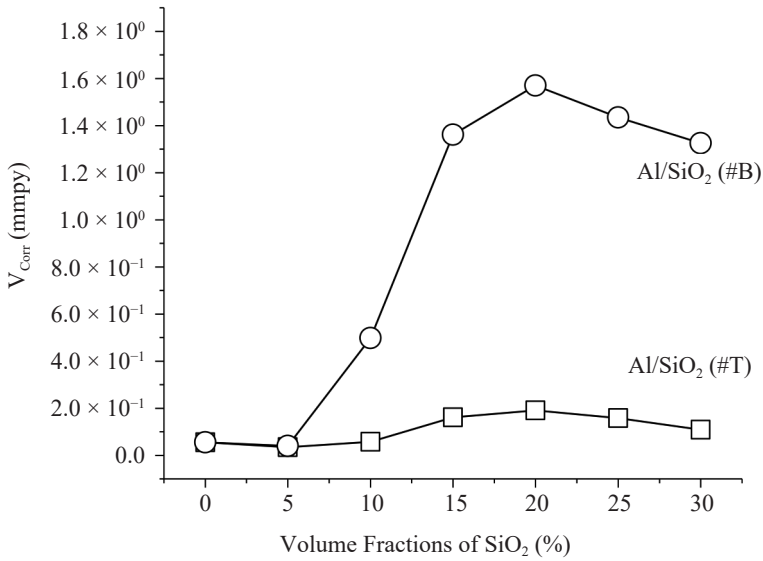

Figure 12: Corrosion rate (V_{Corr}) of Al/SiO_2. T refers to TMAH solution and B refers to the N-butanol solution.

4. CONCLUSION

Al/SiO_2 composites were successfully produced using a simple metallurgical approach and employing commercial Al powders and extracted amorphous SiO_2 powders from Indonesian natural silica sands. From the phase and microstructural evaluations, it was shown that besides crystalline Al and amorphous SiO_2, γ-Al_2O_3 were formed within the composites as had been predicted as the physical consequences of the presence of active solutions and sintering.

The addition of SiO_2 reduced the density or increased the porosity of the composites. Reduction of other physical properties in terms of yield strength and compression strength, ultimate compression strength, and modulus of elasticity were also observed due to the addition of SiO_2. The composite with 5% SiO_2 exhibited the highest values of yield strength, modulus of elasticity and ultimate compression strength. Furthermore, corrosion rates (V_{Corr}) in the case of Al/SiO_2(T) were lower than that of Al/SiO_2(B) composites.

5. ACKNOWLEDGEMENTS

One of the authors (Munasir) is grateful to the Universitas Negeri Surabaya, Institut Teknologi Sepuluh Nopember, and the Ministry of Research, Technology and Higher Education of the Republic of Indonesia (grant number: 170/UN.38.9/HK/LT/2015). Acknowledgement is extended to Bundesanstalt für Materialforschung und-prüfung (BAM), Germany, which has provided author Munasir with the opportunity to study corrosion and conduct research on geothermal and surface treatment of corrosion in geothermal environments.

6. REFFERENCES

1. Halambek, J. et al. (2014). Corrosion behavior of aluminum and AA5754 alloy in 1% acetic acid solution in presence of laurel oil. *Int. J. Electrochem. Sci*., 9(10), 5496–5506.
2. Rattanasak, U., Chindaprasirt, P. & Suwanvitaya, P. (2010). Development of high volume rice husk ash aluminum silicate composites. *Int. J. Miner. Metall. Mater.*,17(5), 654–659, https://doi.org/10.1007/s12613-010-0370-0.
3. Gurcan, A. B. & Baker, T. N. (1995). Wear behavior of AA6061 aluminum alloy and its composites. *Wear*, 188(1–2), 185–191, https://doi.org/10.1016/0043-1648(95)06639-X.
4. Parvin, N. & Rahimian, M. (2012). The characteristics of alumina particle reinforced pure Al matrix composite. *Acta Phys. Polon. A*, 121(1), 108–110, https://doi.org/10.12693/APhysPolA.121.108.
5. Kumar, G. B. V. et al. (2010). Studies on Al6061-SiC and Al7075-Al_2O_3 metal matrix composites. *J. Miner. Mat. Char. Eng.*, 9(1), 43–55, https://doi.org/10.4236/jmmce.2010.91004.
6. Mallikarjuna, G. B. & Basavaraj, E. (2018). Preparation and characterization of aluminium-silica metal matrix composite. *AIP Conf. Proceed.*, 1943(1), 020105, https://doi.org/10.1063/1.5029681.
7. Sayuti, M. et al. (2012). Manufacturing and properties of quartz (SiO_2) particulate reinforced Al-11.8%Si matrix composites: Composites and their properties. *Intech*, 18, 411–436, https://doi.org/10.5772/48095.
8. Rahman, H. M. & Mamun Al-Rashed, H. M. (2014). Characterization of silicon carbide reinforced aluminum matrix composites. *Proced. Eng.*, 90(2014), 103–109, https://doi.org/10.1016/j.proeng.2014.11.821.
9. Casati, R. & Vedani, M. (2014). Metal matrix composites reinforced by nano-particles: A review. *Metals*, 4(2014), 65–83, https://doi.org/10.3390/met4010065.
10. Ravichandran, M., Sait, N. A. & Anandakrishnan, V. (2014). Synthesis and forming behavior of aluminum-based hybrid powder metallurgic composites. *Int. J. Miner. Metall. Mater.*, 21(2), 181–189, https://doi.org/10.1007/s12613-014-0883-z.

11. Zuhailawati, H. P., Samayamutthirian, P. & Haizu, C. H. M. (2007). Fabrication of low cost of aluminum matrix composite reinforced with silica sand. *J. Phys. Sci.*, 18(1), 47–55.
12. Gregolin, E. N. et al. (2004). Co-continuous silica-aluminium composite. *J. Mat. Proc. Tech.*, 157–158, 688–694, https://doi.org/10.1016/j.jmatprotec.2004.07.127.
13. Wang, J. (2008). Mechanical alloying of amorphous Al–SiO_2 powders. *J. Alloys Comp.*, 456(1–2),139–142, https://doi.org/10.1016/j.jallcom.2007.02.027.
14. Rizkalla, H. L. & Abdulwahed, A. (1996). Some mechanical properties of metal-nonmetal Al-SiO_2 particulate composites. *J. Mater. Proc. Tech.*, 56(1–4), 398–403, https://doi.org/10.1016/0924-0136(96)85107-7.
15. Oni, B. O. et al. (2008). Corrosion behavior of tin-plated carbon steel and aluminum in NaCl solutions using electrochemical impedance spectroscopy. *J. Min. Mater. Char. Eng.*, 7(4), 331–346, https://doi.org/10.4236/jmmce.2008.74026.
16. Mansfeld, F. (2005). Tafel slopes and corrosion rates obtained in the pre-Tafel region of polarization curves. *J. Corr. Sci.*, 47(12), 3178–3186, https://doi.org/10.1016/j.corsci.2005.04.012.
17. Li, S. M. et al. (2015). Effect of intermetallic phases on the anodic oxidation and corrosion of 5A06 aluminum alloy. *Int. J. Miner. Metal. Mater.*, 22(2), 167–174, https://doi.org/10.1007/s12613-015-1057-3.
18. Pinto, G. M., Nayak, J. & Shetty, A N. (2009). Corrosion behavior of 6061 Al-15vol. Pct. SiC composite and its base alloy in a mixture of 1:1 hydrochloric and sulphuric acid medium. *Int. J. Electrochem. Sci.*, 4, 1452–1468.
19. Bienias, J. et al. (2003). Microstructure and corrosion behavior of aluminum fly ash composites. *J. Opto. Adv. Mater.*, 5(2), 493–502.
20. Munasir, M. et al. (2015). Synthesis of SiO_2 nanopowders containing quartz and cristobalite phases from silica sands. *Mater. Sci.-Pol.*, 33(1), 47–55, https:/doi.org/10.1515/msp-2015-0008.
21. Fu, S. Y. et al. (2008). Effects of particle size, particle/matrix interface adhesion and particle loading on mechanical properties of particulate–polymer composites. *Comp. B*, 39, 933–941, https://doi.org/10.1016/j.compositesb.2008.01.002.
22. Choren, J. A., Heinrich, S. M. & Silver-Thorn, M. B. (2013). Young's modulus and volume porosity relationships for additive manufacturing applications. *J. Mater. Sci.*, 48(15), 5103–5112, https://doi.org/10.1007/s10853-013-7237-5.
23. Vijayaram, T. R. (2009). Foundry metallurgy of silicon dioxide particulate-reinforced LM6 alloy matrix composite, studies on tensile properties and fractography. *Ind. Found. J.*, 55(2), 21–26.
24. Santos, P. S., Santos, H. S. & Toledo, S.P. (2000). Standard transition aluminas: Electron microscopy studies. *Mater. Res.*, 3(4), 104–114, http://doi.org/10.1590/S1516-14392000000400003.
25. Jiang Y-F. et al. (2018). Insights into the polymorphic transformation mechanism of aluminum hydroxide during carbonation of potassium aluminate solution. *Cryst. Eng. Comm*., 10(20), 1431–1442, https://doi.org/10.1039/C7CE01656E.
26. Gawet, B. & Øye, G. (2013). Hierarchical γ-alumina monoliths with macro-and mesoporosity prepared by using cross-linked dextran gel beads as the template. *Mater. Lett.*, 95(2), 86–88, https://doi.org/10.1016/j.matlet.2012.12.081.

27. Temuujin, J. et al. (2000). Thermal formation of corundum from aluminum hydroxides prepared from various aluminum salts. *Bull. Mater. Sci.*, 23(4), 301–304, https://doi.org/10.1007/BF02720086.
28. Su, X. & Li, Y. (2011). Low-temperature synthesis of single-crystal alpha alumina platelets by calcining bayerite and potassium sulfate. *J. Mater. Sci. Technol.*, 27(11), 1011–1015, https://doi.org/10.1016/S1005-0302(11)60179-5.